# Hexapod PtRuCu Nanocrystalline Alloy for Highly Efficient and Stable Methanol Oxidation

Shengfeng Xue,[†,¶] Wentao Deng,[‡,¶] Fang Yang,[†,¶] Jinlong Yang,[†] Ibrahim Saana Amiinu,[†] Daping He,*[†,§] Haolin Tang,*[†] and Shichun Mu*[†]

[†]State Key Laboratory of Advanced Technology for Materials Synthesis and Processing, Wuhan University of Technology, Wuhan 430070, China

[‡]Department of Chemistry, University of Bath, Claverton Down, Bath BA2 7AY, U.K.

[§]Hubei Engineering Research Center of RF-Microwave Technology and Application, Wuhan University of Technology, Wuhan 430070, China

**S** *Supporting Information*

**ABSTRACT:** A hexapod PtRuCu nanocrystalline alloy material is successfully fabricated by a facile approach based on Stranski−Krastanov growth and galvanic replacement and used as an efficient catalyst for direct methanol fuel cells (DFMCs). Because of the synergetic effect of metallic elements in the methanol oxidation, the activity and durability of the prepared PtRuCu/C catalyst is significantly enhanced. It has a mass activity of 1.35 A $mg_{Pt}^{-1}$ and a specific activity of 3.92 mA $cm^{-2}$, which are 3.8 and 8.2 times higher than those of Pt/C, respectively. Its mass activity only decreases 27% after 800 CV cycles compared with Pt/C (60% decline), indicating the admirable stability of the PtRuCu catalyst.



**KEYWORDS:** *Pt, ternary metallic alloy, methanol oxidation reaction (MOR), hexapod, electrochemical catalysis*
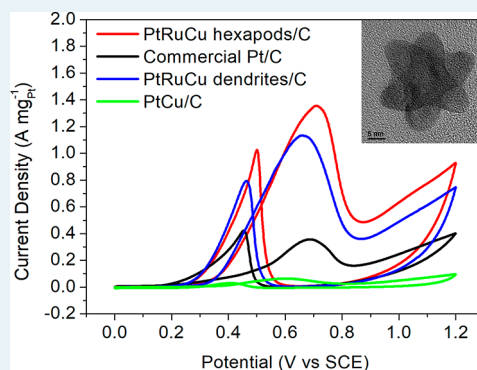
## INTRODUCTION

Direct methanol fuel cells (DMFCs) are promising and efficient devices in the conversion of chemical energy into electric power for portable communication devices and small vehicles because of their high energy density.[1] The application of catalysts has attracted enormous attention in order to increase the efficiency of DMFCs, and of which Pt is found to be an ideal anode catalyst attributed to its distinct electronic properties for methanol oxidation reaction (MOR).[2−4] However, the active sites on pure Pt are easily adsorbed and blocked by intermediate products, impeding further reactions. This poisoning phenomenon is particularly serious in an acidic electrolyte.[4]

Researchers in recent years have worked on developing platinum alloys (PtM, M = Pd,[5] Ru,[6] Cu,[7] Co,[8] Ni,[9] etc.) to avoid the catalyst poisoning, especially the poisoning problem caused by CO and HCOOH, which are produced at the active sites on Pt particles during the MOR reaction. An alloy catalyst could reduce the CO poisoning depending on the properties of the additionally introduced metal element. For example, it has been reported that catalysts based on PtRu alloys show impressive CO tolerance due to the fact that CO can be easily oxidized by the aid of Ru(OH⁻).[10,11] Another catalyst, PtCu also has high electrocatalytic performance as MOR catalyst, owing to the fact that Cu can lower the d band center of Pt, which could protect Pt and its active sites from CO blocking.[12,13]

In addition, alloys with controlled morphologies such as nanowires,[14] nanocages,[15] nanodendrites,[16] nanoframes,[17] or core−shell structures[18] have been employed to minimize Pt loading and maximize the stability and activity of catalysts, especially nanomaterials with distinct 3D structures possess better catalytical activities in virtue of abundant active sites and large specific areas.[19,20] Recently, diversified reagents have been found conducive to synthesize nanoparticles with controlled morphologies or new structures. For instance, CO can play a significant role in constructing Pt nanocubes and meanwhile limiting the growth of PtCu nanoparticles.[21] By the assistance of CO, nanomaterials with special morphologies can be created.[22] Cetyltrimethyl ammonium bromide (CTAB) has also been reported to be a surfactant propitious to form high index facets (HIFs) like Pt(110) or (111) which can improve the catalyst activity and affect reduction rates through ligand effects in metal nanoparticle fabrication.[23,24] Despite the fact that many researchers have developed catalysts with high catalytic efficiency, most of their synthetic methods are complicated.[25,26]
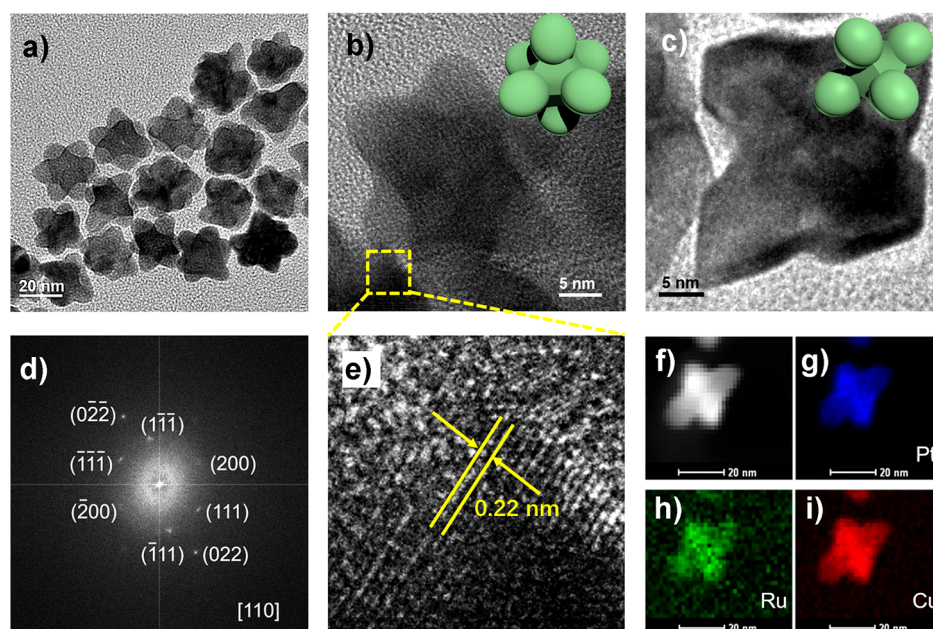
**Figure 1.** (a) TEM images of PtRuCu hexapods; (b,c) HRTEM image of PtRuCu hexapods viewed from two perspectives and their corresponding models as insets; (d) FFT pattern of Figure (b); (e) magnified selected area in Figure (b);(f−i) the corresponding elemental mappings of Pt, Ru, and Cu.

In this work, we report a facile synthesis approach for making ternary PtRuCu alloy nanoparticles with a hexapod structure. In a typical procedure, $Cu(COOH)_2$ was reduced to produce Cu seeds colloidal by the assistance of oleylamine, glucose, and CTAB in the atmosphere of CO. Oleylamine containing $Pt(acac)_2$ and $Ru(acac)_3$ were then added into the colloidal to get PtRuCu alloying nanocrystals (see details in Experimental Section). The electrocatalytic performance of the as-synthesized catalyst was studied in acidic electrolyte containing methanol. The results indicated that the hexapod PtRuCu alloy nanocrystals possessed greatly enhanced performance when used as a methanol oxidation catalyst compared with the commercial Pt/C catalyst.

## ■ EXPERIMENTAL SECTION

**Chemicals and Materials.** Platinum acetylacetonate ($Pt(acac)_2$, 97.0%), ruthenium acetylacetonate ($Ru(acac)_3$, 97.0%), cupric acetate ($Cu(COOH)_2$, 97.0%), oleylamine ($C_{18}H_{37}N$, 80−90%), and cetyltrimethyl ammonium bromide (CTAB, 99%) were all purchased from Macklin, China. Glucose (AR), methanol (AR), absolute ethanol (AR), toluene (AR), and isopropanol (AR) were all supplied by Aldrich. Vulcan XC-72 was purchased from Sigma-Aldrich. Perchloric acid ($HClO_4$, 70−72%) was purchased from Aladdin. Carbon monoxide (CO, 99.5%) was purchased from Beiwen gas factory, China. Nafion solution (5 wt %) was purchased from Sigma-Aldrich. Commercial Pt/C for comparison was purchased from Johnson Matthey. All chemicals were used directly without further purification.

**Synthesis of PtRuCu Alloy.** To prepare the PtRuCu hexapods, $Cu(COOH)_2$ (7.2 mg, 0.04 mmol), glucose (60 mg, 0.3 mmol), and CTAB (73 mg, 0.2 mmol) were dissolved in oleylamine (5 mL, 13 mmol) and sonicated for 30 min to get a homogeneous solution. After a removal of oxygen under vacuum, the solution was heated to 270 °C and kept at this temperature under carbon monoxide atmosphere for 30 min with vigorous stirring. Then, it was cooled down to room

temperature before 5 mL of oleylamine solution containing $Pt(acac)_2$ (20.4 mg, 0.052 mmol) and $Ru(acac)_3$ (3.2 mg, 0.008 mmol) was added. The solution was again heated up to 300 °C and kept for 1 h with stirring. The products were collected by washing under centrifugation at 10 000 rpm with the mixture of toluene and methanol (v/v = 1:1) for at least three times. PtCu alloy was synthesized by the same method in the absence of $Ru(acac)_3$. PtRuCu dendrites were synthesized by the same method except changing the holding time at 300 °C from 1 to 2 h.

**Materials Characterization.** Morphologies of PtRuCu alloy were carried out by a transmission electron microscopy (TEM) (JEM-2100F STEM/EDS, JEOL, Japan) operated at 200 kV. Powder X-ray diffraction (XRD) was tested on an X-ray diffractometer (D/MAX-RB, Rigaku, Japan) with a Cu Kα X-ray source ($\lambda$ = 1.530598 Å). The content of each element in the catalyst was determined by Inductive Coupled Plasma Optical Emission Spectrometer (ICP-OES) (Prodigy 7, Teledyne Leeman Laboratories). X-ray photoelectron spectroscopy (XPS) measurements were performed by ESCALAB 250Xi.

**Electrochemical Measurements.** The electrochemistry measurements were carried out by using a three-electrode system on an electrochemical workstation (CHI 760E, Chenhua Co., Shanghai, China). A glassy carbon electrode (GCE, 5 mm diameter), a saturated calomel electrode (SCE), and a platinum wire were used as the working electrode, the reference electrode, and the counter electrode, respectively. The as-synthesized PtRuCu alloy was mixed with Vulcan XC-72 (nanoparticle to carbon w/w = 20/80) in 10 mL ethanol aqueous solution (90 vol %). The slurry was sonicated for an hour before centrifugation. The sediment was collected and dried at 80 °C in a drying box for 12 h to prepare the catalyst labeled as PtRuCu/C. Five mg PtRuCu/C was mixed with 1000 $\mu$L of isopropanol aqueous solution (90 vol %) and 20 $\mu$L of Nafion solution (5 wt %) to prepare the ink for
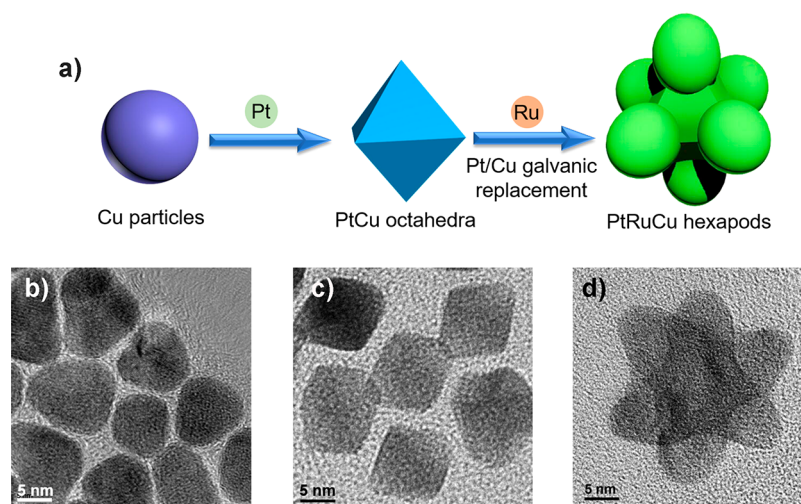
**Figure 2.** (a) Structure evolution from Cu particles to PtRuCu hexapods and (b−d) corresponding TEM images for Cu particles, PtCu octahedra, and PtRuCu hexapods.
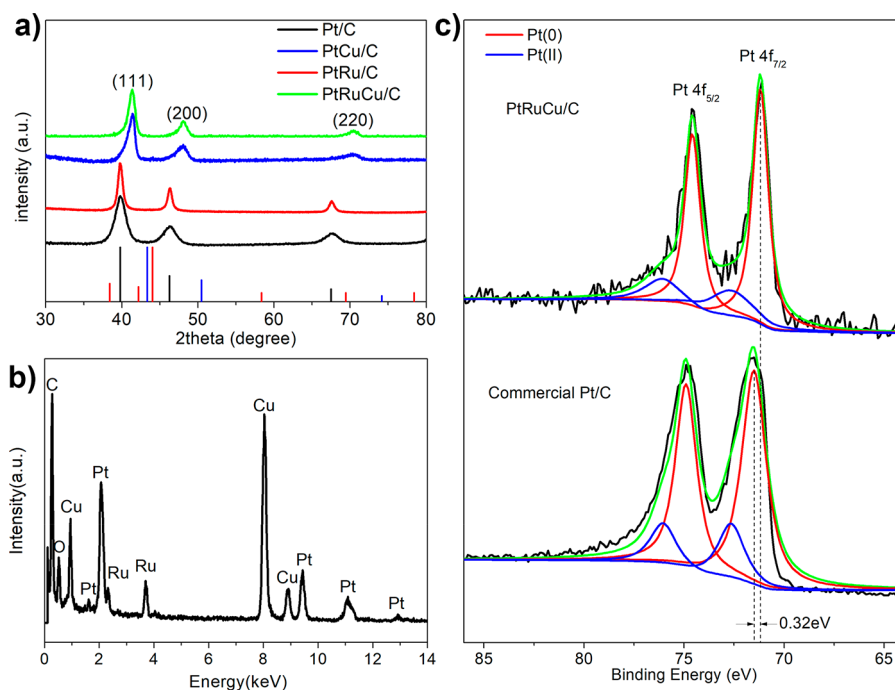


**Figure 3.** (a) XRD patterns of Pt/C, PtRu/C, PtCu/C, and PtRuCu(hexapods)/C. PDF cards of Pt (JCPDS: 04-0802, black), Ru (JCPDS: 06-0663, red) and Cu (JCPDS: 48-1549, blue) are as illustrated below the XRD patterns; (b) EDS spectrum of PtRuCu hexapods; (c) XPS spectra in Pt 4f region for PtRuCu/C and commercial Pt/C.

electrochemistry measurements. Five microliters of ink was dropped on the electrode for each measurement.

Cyclic voltammogram (CV) measurements were carried out in a three-electrode system with 0.1 M HClO$_4$ as the electrolyte at a scan rate of 50 mV s$^{-1}$, and the potential window is from −0.3 V to 0.9 V. Before the measurements, the electrolyte was blown with nitrogen for 20 min.

Methanol oxidation reaction (MOR) curves were also obtained in 1 M methanol and 0.1 M HClO$_4$ by cyclic voltammogram in a three-electrode system as mentioned above. The system was scanned at 50 mV s$^{-1}$ in the potential range from 0 to 1.2 V. Electrolyte used was bubbled with nitrogen before and during the MOR measurements.

CO stripping curves were obtained in 0.1 M HClO$_4$. Before each measurement, CO was bubbled into the electrolytic cell for 10 min. Then the potential of the working electrode was hold at 0.1 V vs reversible hydrogen electrode (RHE) for 10 min via $i-t$ technique to make CO adsorbed on the catalyst. After that, CO was removed from the electrolyte by bubbling N$_2$ for 30 min. Then CO stripping curves were recorded at a scan rate of 50 mV/s between 0.05 and 1.2 V vs RHE.

## ■ RESULTS AND DISCUSSION

As shown in Figure 1a−c, the hexapod PtRuCu nanocrystal particles with six identical arms can be identified by transmission electron microscopy (TEM). They can be regarded as an octahedral structure with six islands on each
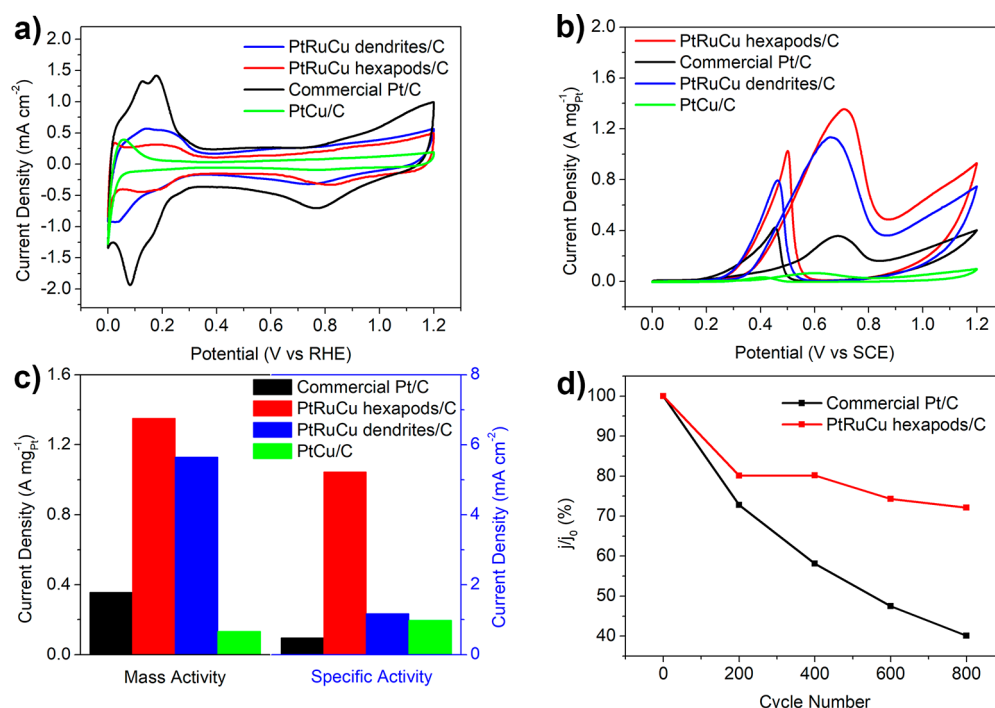
**Figure 4.** Electrocatalytic activity and stability performances of PtRuCu hexapods/C (PtRuCu/C), PtRuCu dendrites/C, PtCu/C, and commercial Pt/C. (a) CV curves in 0.1 M $HClO_4$; (b) Mass activity in 0.1 M $HClO_4$ + 1 M $CH_3OH$ solution for commercial Pt/C, PtRuCu hexapods/C (PtRuCu/C), PtRuCu dendrites/C, and PtCu/C, respectively; (c) MOR mass activity and specific activity in 0.1 M $HClO_4$ + 1 M $CH_3OH$ solution for commercial Pt/C, PtRuCu hexapods/C (PtRuCu/C), PtRuCu dendrites/C and PtCu/C; (d) MOR durability comparison of commercial Pt/C and PtRuCu hexapods/C (PtRuCu/C).

corner. More evidence can be found in the structure evolution observed through TEM images (Figure 2). In addition, the Fast Fourier Transform (FFT) pattern (Figure 1d) shows regularly arranged spots, indicating that the PtRuCu hexapods is presented in a single crystal with the (111) facets. As shown in Figure 1a, such particles have a size range of 26−30 nm based on TEM observation, and the average size is about 28 nm. As shown in the high-resolution TEM images (Figure 1e), the spacing of the lattice fringes of PtRuCu nanoparticles is 0.22 nm, corresponding to PtCu (111) facet.[27] Elemental mappings of the product manifested that Pt, Ru, and Cu are uniformly distributed in the hexapod PtRuCu particles (Figure 1f−i).

The structure evolution from Cu particles to PtRuCu hexapods is illustrated in Figure 2. As described in the experimental part, the reactions correspond to two stages. Copper particles were first obtained through reduction of $Cu(OAc)_2$ (Figure 2a). At the second stage which relates to the Stranski−Krastanov growth and galvanic replacement,[5] the reaction time was found to be of great importance in determining the composition and morphology of the product. When the reaction system was kept for 30 min at 300 °C after the addition of $Pt(acac)_2$ and $Ru(acac)_3$ (noting that the Pt and Ru precursors were added at the same time), the resulting product was octahedral (Figure 2c) rather than the hexapods (Figure 2d). When $Pt(acac)_2$ and $Ru(acac)_3$ were added into the reaction system, $Pt(acac)_2$ was reduced to Pt, and PtCu octahedra were then constructed.[27,28] This process is prior to the reduction of $Ru(acac)_3$ because of the more positive reduction potential of $Pt^{II}$. With the proceeding of the reaction, $Pt^{II}$ and $Ru^{III}$ were both reduced and then constructed a skin on PtCu octahedra on the basis of a layer-by-layer mechanism (epitaxial growth). However, the standard potential of $Pt^{II}/Pt$

pair (1.18 V) are more positive than that of $Cu^{II}/Cu$ pair (0.34 V), giving rise to a galvanic replacement between $Pt^{II}$ and Cu, and it then results in the presence of Pt and Ru atoms in the core of the hexapods according to the elemental maps of PtRuCu hexapods.[29] When the reaction time was sufficient (i.e., 60 min in this work), Cu (reduced from $Cu^{II}$ being replaced in the presence of Pt atoms), Pt, and Ru started preferential growth at six vertices of the octahedra and formed PtRuCu hexapods with octahedra cores. Simultaneously, the galvanic replacement was still continuing, which was the main reason that the distribution of Pt was basically the same as that of Cu in elemental maps. However, when the reaction time was extended to 2 h, the PtRuCu hexapods would grow into crystals with more complex morphologies like dendrites (Figure S1).

The alloy was further investigated by powder X-ray diffraction (XRD) measurement to understand the phase and crystal information. The obtained XRD patterns of Pt/C, PtCu/C, PtRu/C, and PtRuCu/C are shown in Figure 3a. It is observed that the peaks of PtRuCu shift to higher angles compared with pure Pt (JCPDS: 04-0802), indicating that Pt has been alloyed with other metals. The XRD pattern of PtRuCu is similar to that of PtCu, but slightly shifts toward the peaks of PtRu. The Peaks located at 41.4°, 48.1°, and 70.6° can be assigned to (111), (200), and (220) facets of PtCu, respectively.[30] The XRD pattern of PtRuCu dendrites were also measured and the dendrites show a similar crystal structure with PtRuCu hexapods (Figure S2). Noting that no Ru phase was detected in XRD patterns in both PtRu and PtRuCu due to the detection limit of XRD measurement. To prove the existence of Ru in the alloy, energy-dispersive spectrometry (EDS) and TEM elemental mapping were employed and confirmed the existence of Ru (Figure 1f and

Figure 3b), and Ru accounts for 0.5 at% in the alloy, identified by ICP-OES. The content of Pt and Cu was also measured to be 51.5 at% and 48 at%. As shown in Figure 3c, the XPS spectrum of Pt in 4f regions can be decomposed into two groups of peaks: Pt (0) (71.18 and 74.58 eV) and Pt (II) (72.98 and 76.38 eV, listed in Table S1). Significantly, the Pt (0) peak of PtRuCu/C located at 71.18 eV (4f 5/2) shows a 0.32 eV negative shift in comparison with the commercial Pt/C (71.50 eV). In the Cu 2p spectrum, peaks located at 952.66 eV (Cu 2p 1/2) and 932.80 eV (Cu 2p 3/2) indicate the presence of Cu (Figure S3), and the positive shifts of Cu 2p peaks compared with metallic Cu indicate the decline of Cu electron density and a downshift of the d-band center of Pt, which is beneficial for the catalytic activity.[31,32] Both Ru 3d and Ru 3p peaks are shown in Figure S4. It is difficult to distinguish the peaks of Ru 3d peak and C 1s (Figure S4a) because the Ru 3d peak is close to C 1s peak, and the content of Ru is rather low (0.5%). However, Ru can be observed via XPS spectra in the Ru 3p region, which is shown in Figure S4b. An evolution of composition change has been illustrated by XPS spectra (Figure S5) in which the element and content information from Cu particles, PtCu octahedra to PtRuCu hexapods are exhibited.

To compare the electrocatalytic performances of as-synthesized catalyst to the commercial Pt/C, cyclic voltammetry(CV) and methanol electrooxidation experiments were conducted. From the CV curves in Figure 4a, the electrochemical active surface area (ECSA) of the three catalysts were determined to be 34.57 $m^2/g_{Pt}^{-1}$ (PtRuCu hexapods/C), 52.28 $m^2/g_{Pt}^{-1}$ (PtRuCu dendrites/C), 13.3 $m^2/g_{Pt}^{-1}$(PtCu/C), and 74.62 $m^2/g_{Pt}^{-1}$(Pt/C). Compared with commercial Pt/C, the decreased ECSA of PtRuCu/C can be ascribed to the large sizes of metallic nanoparticles.[20]

The prepared PtRuCu trimetallic catalyst shows impressive electrocatalytic performance. When used for methanol oxidation reaction (MOR), as displayed in Figure 4b, the PtRuCu/C catalyst owns nearly a 3-fold mass activity (1.35A mg $_{Pt}^{-1}$) over the commercial Pt/C catalyst (0.47A mg$_{Pt}^{-1}$). Moreover, as shown in Figure 4c, it exhibits a higher specific activity than the commercial Pt/C (5.22 vs. 0.59 mA cm$^{-2}$) and a better activity than the PtRuCu dendrites/C catalyst (1.35 A mg $_{Pt}^{-1}$ vs 1.13 A mg $_{Pt}^{-1}$). The activity difference is partly caused by the different morphologies between them. As the PtRuCu hexapods were not completely grown, therefore, some high index facets (such as Pt (111) on PtCu octahedra) on the alloy were still exposed. This helps to enhance the catalysis activity. As another important index, the ratio of $I_f$ (forward current) to $I_b$ (backward current) can be used to estimate the tolerance of the catalyst to the poisoning of intermediate carbonaceous species such as CO, HCHO and HCOOH.[27] The ratio calculated from Figure 4b indicates that PtRuCu/C ($I_f/I_b$ = 1.32) has better durability (anti-CO poisoning capability) than commercial Pt/C ($I_f/I_b$ = 0.84). In addition, after hundreds of CV cycles, PtRuCu/C and commercial Pt/C catalyst display relatively different stability behaviors (Figure S6). The activity of PtRuCu/C degraded in a much slower rate after the first 200 CV cycles than the commercial Pt/C, and eventually its activity only decreased 27% after 800 CV cycles, which is much better than that of Pt/C (60% decreased, as exhibited in Figure 4d and Figure S6). Interestingly, after 800 CV cycles, the PtRuCu dendrites/C also shows high stability with only 18% decays for MOR catalytic activity (Figure S6c). Notably, PtRuCu/C maintains

higher $I_f/I_b$ ratio compared with commercial Pt/C (1.27 vs 1.10) at the 800th CV scan, suggesting that PtRuCu is still tolerant to CO poisoning even after hundreds of CV cycles (Figure S7).

We further investigated the CO tolerance of PtRuCu/C, PtRu/C, and Pt/C catalysts by CO stripping test in 0.1 M HClO$_4$ at a scan rate of 50 mV/s. The CO stripping curves are shown in Figure 5. The CO stripping peak of PtRuCu/C (0.85
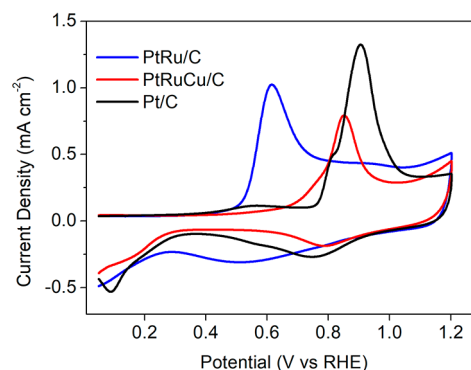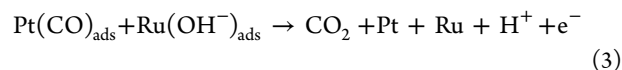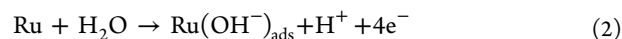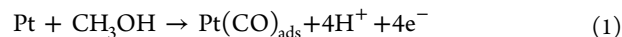


**Figure 5.** CO stripping curves of commercial Pt/C, commercial PtRu/C, and PtRuCu hexapods/C in 0.1 M HClO$_4$.

V) locates at a lower potential than that of Pt/C (0.91 V), indicating a higher CO tolerance of PtRuCu/C catalyst than that of Pt/C. The commercial PtRu/C catalyst shows the lowest peak potential (0.61 V) because of the higher Ru content (~20 wt %).

The good MOR activity and stability of PtRuCu hexapods can be attributed to the synergetic effects of the three metallic elements in the alloy. As a single element catalyst, Pt suffers from poisoning problem. However, introducing other elements to produce Pt-containing alloy can significantly reduce the impacts of poisoning. It has been reported that the formation of Ru(OH$^-$) in the reaction catalyzed by PtRu alloy can improve the stability of the catalyst. The Ru-based catalyst is excellent for methanol oxidation resulting from following reactions:[33]

$$Pt + CH_3OH \rightarrow Pt(CO)_{ads} + 4H^+ + 4e^- \qquad (1)$$

$$Ru + H_2O \rightarrow Ru(OH^-)_{ads} + H^+ + 4e^- \qquad (2)$$

$$Pt(CO)_{ads} + Ru(OH^-)_{ads} \rightarrow CO_2 + Pt + Ru + H^+ + e^- \qquad (3)$$

This mechanism indicates that the existence of Ru, which is prone to form Ru(OH)$_{ads}$, can facilitate the oxidation of CO. Therefore, CO poisoning of active sites on Pt can be reduced. It is also discovered that the onset potential of PtRuCu/C is 0.22 V, lower than that of commercial Pt/C (0.31 V), which manifests that CO can be removed from active sites on Pt at a lower potential after being oxidized by Ru(OH$^-$) (Figure 4b).[26]

In addition to Ru, introduction of Cu into the alloy is also beneficial to the antipoisoning capability. When alloyed with Cu, Pt can achieve a modified d-band by a ligand and strain effect to maintain a constant d-band filling, and consequently, electron structures and chemical properties can be changed on the surface of the alloy.[34−36] Subsurface 3d transition metal atoms improve the broadening of d-band on the Pt surface by the interactions between Pt atoms and Cu atoms; thus, the

average d-band energy can be decreased. This is conducive to the desorption of CO produced in the methanol oxidation reaction at the active sites on Pt, and therefore, the durability of the catalyst can be enhanced.[12,37] Furthermore, Cu atoms on the surface of PtRuCu alloy can be sacrificed to relieve Pt from dissolution, and the activity and durability of PtRuCu/C can be improved in acidic electrolytes. The combination of the fact that $Ru(OH)_{ads}$ can relieve Pt from poisoned by CO and the synergetic effect between Pt and Cu is believed to be the major contribution of enhanced MOR activity of the catalyst.

## ■ CONCLUSIONS

In summary, by using a facile method, we synthesized a PtRuCu alloy with a hexapod structure for robust methanol oxidation catalytic performance. The ternary alloy hexapods were formed by the combination of Stranski−Krastanov growth and galvanic replacement. For the methanol oxidation reaction (MOR), the fabricated PtRuCu/C catalyst exhibits 3.8-fold mass activity, 8.2-fold specific activity, and increased durability compared with the commercial Pt/C catalyst. The reaction time is a crucial factor to obtain an alloy with well-defined morphology and robust activity. This promising catalyst is attributed to the synergetic effect of Pt, Ru, and Cu components. $Ru(OH)_{ads}$ formed in the reactions speeds up the oxidation of CO, and Cu doping could decorate the d-band and decrease the d-band energy of Pt. Therefore, the activity and stability of the Pt-based catalyst are both enhanced.

## ■ ASSOCIATED CONTENT

### ⑤ Supporting Information

The Supporting Information is available free of charge on the ACS Publications website at DOI: 10.1021/acscatal.8b00366.

> TEM images and XRD patterns of PtRuCu dendrites; XPS spectra of PtRuCu, PtCu and Cu; and MOR performances after different CV cycles of Pt/C, PtRuCu/C and PtRuCu dendrites/C; Catalyst durability of commercial Pt/C and PtRuCu/C; and the reaction devices used in the synthesis (PDF)

## ■ AUTHOR INFORMATION

### Corresponding Authors
*E-mail: hedaping@whut.edu.cn.
*E-mail: tanghaolin2005@yahoo.com.cn.
*E-mail: msc@whut.edu.cn.

### ORCID ⓖ
Ibrahim Saana Amiinu: 0000-0003-4426-7893
Daping He: 0000-0002-0284-4990
Shichun Mu: 0000-0003-3902-0976

### Author Contributions
¶S.X., W.D., and F.Y. contributed equally to this work.

### Notes
The authors declare no competing financial interest.

## ■ REFERENCES

(1) Ganesan, R.; Lee, J. S. Tungsten Carbide Microspheres as a Noble-Metal-Economic Electrocatalyst for Methanol Oxidation. *Angew. Chem.* **2005**, *117*, 6715−6718.

(2) Huang, H.; Ma, L.; Tiwary, C. S.; Jiang, Q.; Yin, K.; Zhou, W.; Ajayan, P. M. Worm-Shape Pt Nanocrystals Grown on Nitrogen-Doped Low-Defect Graphene Sheets: Highly Efficient Electrocatalysts for Methanol Oxidation Reaction. *Small* **2017**, *13*, 1603013.

(3) Huang, M.; Zhang, J.; Wu, C.; Guan, L. Pt Nanoparticles Densely Coated on $SnO_2$-Covered Multiwalled Carbon Nanotubes with Excellent Electrocatalytic Activity and Stability for Methanol Oxidation. *ACS Appl. Mater. Interfaces* **2017**, *9*, 26921−26927.

(4) Zhao, X.; Yin, M.; Ma, L.; Liang, L.; Liu, C.; Liao, J.; Lu, T.; Xing, W. Recent Advances in Catalysts for Direct Methanol Fuel Cells. *Energy Environ. Sci.* **2011**, *4*, 2736−2753.

(5) Xiong, Y.; Ma, Y.; Li, J.; Huang, J.; Yan, Y.; Zhang, H.; Wu, J.; Yang, D. Strain-induced Stranski-Krastanov Growth of Pd@Pt Core-shell Hexapods and Octapods as Electrocatalysts for Methanol Oxidation. *Nanoscale* **2017**, *9*, 11077−11084.

(6) Lin, Z.; Chen, W.; Jiang, Y.; Bian, T.; Zhang, H.; Wu, J.; Wang, Y.; Yang, D. Facile Synthesis of Ru-decorated Pt Cubes and Icosahedra as Highly Active Electrocatalysts for Methanol Oxidation. *Nanoscale* **2016**, *8*, 12812−12818.

(7) Nosheen, F.; Zhang, Z. C.; Zhuang, J.; Wang, X. One-pot Fabrication of Single-crystalline Octahedral Pt-Cu Nanoframes and Their Enhanced Electrocatalytic Activity. *Nanoscale* **2013**, *5*, 3660−3663.

(8) Bai, S.; Shao, Q.; Feng, Y.; Bu, L.; Huang, X. Highly Efficient Carbon Dioxide Hydrogenation to Methanol Catalyzed by Zigzag Platinum-Cobalt Nanowires. *Small* **2017**, *13*, 1604311.

(9) Chen, C.; Kang, Y.; Huo, Z.; Zhu, Z.; Huang, W.; Xin, H. L.; Snyder, J. D.; Li, D.; Herron, J. A.; Mavrikakis, M.; Chi, M.; More, K. L.; Li, Y.; Markovic, N. M.; Somorjai, G. A.; Yang, P.; Stamenkovic, V. R. Highly Crystalline Multimetallic Nanoframes with Three-dimensional Electrocatalytic Surfaces. *Science* **2014**, *343*, 1339−1343.

(10) Watanabe, M.; Motoo, S. Electrocatalysis by Ad-atoms: Part II. Enhancement of the Oxidation of Methanol on Platinum by Ruthenium Ad-atoms. *J. Electroanal. Chem. Interfacial Electrochem.* **1975**, *60*, 267−273.

(11) Alayoglu, S.; Nilekar, A. U.; Mavrikakis, M.; Eichhorn, B. Ru-Pt Core-shell Nanoparticles for Preferential Oxidation of Carbon Monoxide in Hydrogen. *Nat. Mater.* **2008**, *7*, 333−338.

(12) Papadimitriou, S.; Armyanov, S.; Valova, E.; Hubin, A.; Steenhaut, O.; Pavlidou, E.; Kokkinidis, G.; Sotiropoulos, S. Methanol Oxidation at Pt-Cu, Pt-Ni, and Pt-Co Electrode Coatings Prepared by a Galvanic Replacement Process. *J. Phys. Chem. C* **2010**, *114*, 5217−5223.

(13) Hunt, S. T.; Milina, M.; Alba-Rubio, A. C.; Hendon, C. H.; Dumesic, J. A.; Román-Leshkov, Y. Self-assembly of Noble Metal Monolayers on Transition Metal Carbide Nanoparticle Catalysts. *Science* **2016**, *352*, 974−978.

(14) Liao, Y.; Yu, G.; Zhang, Y.; Guo, T.; Chang, F.; Zhong, C. Composition-Tunable PtCu Alloy Nanowires and Electrocatalytic Synergy for Methanol Oxidation Reaction. *J. Phys. Chem. C* **2016**, *120*, 10476−10484.

(15) Zhang, L.; Roling, L. T.; Wang, X.; Vara, M.; Chi, M.; Liu, J.; Choi, S. I.; Park, J.; Herron, J. A.; Xie, Z.; Mavrikakis, M.; Xia, Y. Platinum-based Nanocages with Subnanometer-thick Walls and Well-defined, Controllable Facets. *Science* **2015**, *349*, 412−416.

(16) Lu, S.; Eid, K.; Ge, D.; Guo, J.; Wang, L.; Wang, H.; Gu, H. One-pot Synthesis of PtRu Nanodendrites as Efficient Catalysts for Methanol Oxidation Reaction. *Nanoscale* **2017**, *9*, 1033−1039.

(17) Ye, W.; Chen, S.; Ye, M.; Ren, C.; Ma, J.; Long, R.; Wang, C.; Yang, J.; Song, L.; Xiong, Y. $Pt_4PdCu_{0.4}$ Alloy Nanoframes as Highly Efficient and Robust Bifunctional Electrocatalysts for Oxygen Reduction Reaction and Formic Acid Oxidation. *Nano Energy* **2017**, *39*, 532−538.

(18) Strasser, P.; Koh, S.; Anniyev, T.; Greeley, J.; More, K.; Yu, C.; Liu, Z.; Kaya, S.; Nordlund, D.; Ogasawara, H.; Toney, M. F.; Nilsson, A. Lattice-strain Control of the Activity in Dealloyed Core-shell Fuel Cell Catalysts. *Nat. Chem.* **2010**, *2*, 454−460.

(19) Ding, J.; Bu, L.; Guo, S.; Zhao, Z.; Zhu, E.; Huang, Y.; Huang, X. Morphology and Phase Controlled Construction of Pt−Ni

Nanostructures for Efficient Electrocatalysis. *Nano Lett.* **2016**, *16*, 2762−2767.

(20) Xia, B. Y.; Wu, H. B.; Wang, X.; Lou, X. W. One-Pot Synthesis of Cubic $PtCu_3$ Nanocages with Enhanced Electrocatalytic Activity for the Methanol Oxidation Reaction. *J. Am. Chem. Soc.* **2012**, *134*, 13934−13937.

(21) Wu, B.; Zheng, N.; Fu, G. Small Molecules Control the Formation of Pt Nanocrystals: a Key Role of Carbon Monoxide in the Synthesis of Pt Nanocubes. *Chem. Commun.* **2011**, *47*, 1039−1041.

(22) Dai, L.; Mo, S.; Qin, Q.; Zhao, X.; Zheng, N. Carbon Monoxide-Assisted Synthesis of Ultrathin $PtCu_3$ Alloy Wavy Nanowires and Their Enhanced Electrocatalysis. *Small* **2016**, *12*, 1572−1577.

(23) Xie, S.; Lu, N.; Xie, Z.; Wang, J.; Kim, M. J.; Xia, Y. Synthesis of Pd-Rh Core-frame Concave Nanocubes and Their Conversion to Rh Cubic Nanoframes by Selective Etching of the Pd Cores. *Angew. Chem., Int. Ed.* **2012**, *51*, 10266−10270.

(24) Qi, Y.; Bian, T.; Choi, S. I.; Jiang, Y.; Jin, C.; Fu, M.; Zhang, H.; Yang, D. Kinetically Controlled Synthesis of Pt-Cu Alloy Concave Nanocubes with High-index Facets for Methanol Electro-oxidation. *Chem. Commun.* **2014**, *50*, 560−562.

(25) Ma, S. Y.; Li, H. H.; Hu, B. C.; Cheng, X.; Fu, Q. Q.; Yu, S. H. Synthesis of Low Pt-Based Quaternary PtPdRuTe Nanotubes with Optimized Incorporation of Pd for Enhanced Electrocatalytic Activity. *J. Am. Chem. Soc.* **2017**, *139*, 5890−5895.

(26) Tiwari, J. N.; Lee, W. G.; Sultan, S.; Yousuf, M.; Harzandi, A. M.; Vij, V.; Kim, K. S. High-Affinity-Assisted Nanoscale Alloys as Remarkable Bifunctional Catalyst for Alcohol Oxidation and Oxygen Reduction Reactions. *ACS Nano* **2017**, *11*, 7729−7735.

(27) Zhang, J.; Yang, H.; Martens, B.; Luo, Z.; Xu, D.; Wang, Y.; Zou, S.; Fang, J. Pt-Cu Nanoctahedra: Synthesis and Comparative Study with Nanocubes on Their Electrochemical Catalytic Performance. *Chem. Sci.* **2012**, *3*, 3302−3306.

(28) Jia, Y.; Su, J.; Chen, Z.; Tan, K.; Chen, Q.; Cao, Z.; Jiang, Y.; Xie, Z.; Zheng, L. Composition-Tunable Synthesis of Pt−Cu Octahedral Alloy Nanocrystals from PtCu to $PtCu_3$ via Underpotential-deposition-like Process and Their Electro-catalytic Properties. *RSC Adv.* **2015**, *5*, 18153−18158.

(29) Ding, J.; Zhu, X.; Bu, L.; Yao, J.; Guo, J.; Guo, S.; Huang, X. Highly Open Rhombic Dodecahedral PtCu Nanoframes. *Chem. Commun.* **2015**, *51*, 9722−9725.

(30) Chen, W.; Sun, G.; Liang, Z.; Mao, Q.; Li, H.; Wang, G.; Xin, Q.; Chang, H.; Pak, C.; Seung, D. The Stability of a PtRu/C Electrocatalyst at Anode Potentials in a Direct Methanol Fuel Cell. *J. Power Sources* **2006**, *160*, 933−939.

(31) Crist, B. V. BE Lookup Table for Signals from Elements and Common Chemical Species. *Handbook of Monochromatic XPS Spectra: The Elements of Native Oxides*; Wiley: Chichester, U.K., 1999, *1*, 77, 358.

(32) Li, C.; Liu, T.; He, T.; Ni, B.; Yuan, Q.; Wang, X. Composition-driven Shape Evolution to Cu-rich PtCu Octahedral Alloy Nanocrystals as Superior Bifunctional Catalysts for Methanol Oxidation and Oxygen Reduction Reaction. *Nanoscale* **2018**, *10*, 4670−4674.

(33) Siller-Ceniceros, A. A.; Sánchez-Castro, M. E.; Morales-Acosta, D.; Torres-Lubian, J. R.; Martínez, G. E.; Rodríguez-Varela, F. J. Innovative Functionalization of Vulcan XC-72 with Ru Organometallic Complex: Significant Enhancement in Catalytic Activity of Pt/C Electrocatalyst for the Methanol Oxidation Reaction (MOR). *Appl. Catal., B* **2017**, *209*, 455−467.

(34) Kitchin, J. R.; Norskov, J. K.; Barteau, M. A.; Chen, J. G. Role of Strain and Ligand Effects in the Modification of the Electronic and Chemical Properties of Bimetallic Surfaces. *Phys. Rev. Lett.* **2004**, *93*, 156801.

(35) Moseley, P.; Curtin, W. A. Computational Design of Strain in Core-Shell Nanoparticles for Optimizing Catalytic Activity. *Nano Lett.* **2015**, *15*, 4089−4095.

(36) Asano, M.; Kawamura, R.; Sasakawa, R.; Todoroki, N.; Wadayama, T. Oxygen Reduction Reaction Activity for Strain-Controlled Pt-Based Model Alloy Catalysts: Surface Strains and Direct Electronic Effects Induced by Alloying Elements. *ACS Catal.* **2016**, *6*, 5285−5289.

(37) Kitchin, J. R.; Norskov, J. K.; Barteau, M. A.; Chen, J. G. Modification of The Surface Electronic and Chemical Properties of Pt(111) by Subsurface 3d Transition Metals. *J. Chem. Phys.* **2004**, *120*, 10240−10246.